

# *Ab initio* predictions for *polarized* DT thermonuclear fusion

Guillaume Hupin<sup>1,2,3</sup>, Sofia Quaglioni<sup>3</sup> and Petr Navrátil<sup>4</sup>

<sup>1</sup> Institut de Physique Nucléaire, IN2P3/CNRS, Université Paris-Sud, Université Paris-Saclay, F-91406 Orsay Cedex, France

<sup>2</sup> CEA, DAM, DIF, F-91297 Arpajon, France

<sup>3</sup> Lawrence Livermore National Laboratory, P.O. Box 808, L-414, Livermore, California 94551, USA

<sup>4</sup> TRIUMF, Vancouver, BC V6T2A3, Canada

## Abstract

The fusion of deuterium (D) with tritium (T) is the most promising of the reactions that could power the thermonuclear reactors of the future. Already favored for its low activation energy and high yield, it may lead to even more efficient energy generation if obtained in a polarized state, i.e. with the spin of the reactants aligned. While the DT fusion rate has been measured extensively, very little is known of the effects of polarization. Meanwhile, arriving at a fundamental understanding of the fusion process in terms of the laws of quantum mechanics and the underlying theory of the strong force has been a daunting challenge. We use nuclear forces derived from chiral effective field theory and apply the *ab initio* reaction method known as no-core shell model with continuum to predict, for the first time from first principles, the enhancement factor of the polarized DT fusion rate and anisotropy of the emitted neutron and  $\alpha$  particle.

## Article

### Introduction

Thermonuclear reaction rates of light nuclei are critical to nuclear science applications ranging from the modeling of big-bang nucleosynthesis and the early phases of stellar burning to the exploration of nuclear fusion as a terrestrial source of energy. The low-energy regime (tens to hundreds of keV) typical of nucleosynthesis and fusion plasmas is challenging to probe due to low counting rates and the screening effect of electrons, which in a laboratory are bound to the reacting nuclei. A predictive understanding of thermonuclear reactions is therefore needed alongside experiments to achieve the accuracy and/or provide part of the nuclear data required by these applications. A salient example is the fusion of deuterium (D) with tritium ( $^3\text{H}$  or T) to generate a  $^4\text{He}$  nucleus ( $\alpha$ -particle), a neutron and 17.6 MeV of energy released in the form of kinetic energy of the products. This reaction, used at facilities such as ITER<sup>1</sup> and NIF<sup>2</sup> in the pursuit of sustained fusion-energy production, is characterized by a pronounced resonance at the center-of-mass (c.m.) energy of 65 keV above the free D and T nuclei due to the formation of the  $J = 3/2^+$  resonance of the unbound  $^5\text{He}$  nucleus. Fifty years ago, it was estimated<sup>3</sup> that, in the ideal scenario in which the spins of the reactants are perfectly aligned in a total-spin  $3/2$  configuration and assuming that the reaction is isotropic, one could achieve an enhancement of the cross section by a factor of  $\delta = 1.5$ , thus improving the economics of fusion energy

generation<sup>4</sup>. However, while the unpolarized cross section and some analyzing-power data exist, no correlation coefficients have been measured yet to confirm this prediction<sup>5</sup>. More generally, what little is known about the properties of the polarized DT fusion was inferred from measurements of the D<sup>3</sup>He reaction<sup>6</sup>. We report on *ab initio* predictions for the polarized DT fusion using validated nuclear interactions derived in the framework of chiral effective field theory (EFT)<sup>7,8</sup>.

The DT fusion is a primary example of a thermonuclear reaction in which the conversion of two lighter elements to a heavier one occurs through the transfer of a nucleon from the projectile (D) to the target (T). Despite the fairly small number of nucleons involved in this process, arriving at a comprehensive understanding – in terms of the laws of quantum mechanics and the underlying theory of the strong force (quantum chromodynamics) – of the interweaving of nuclear shell structure and reaction dynamics giving rise to the DT fusion already represents a formidable challenge for nuclear theory. We work in the framework of chiral effective field theory (EFT), a powerful tool that enables the organization of the interactions among protons and neutrons in a systematically improvable expansion linked to the fundamental theory of quantum chromodynamics. Specifically, we start from a five-nucleon Hamiltonian including nucleon-nucleon (NN)<sup>9</sup> and three-nucleon (3N)<sup>10-13</sup> interactions at the fourth and third order of chiral EFT, respectively. We then solve the quantum-mechanical five-nucleon problem using the no-core shell model with continuum (NCSMC)<sup>14</sup>. The wave function is obtained by combining conventional static solutions for the aggregate <sup>5</sup>He system<sup>15</sup> with continuous ‘microscopic-cluster’ states made of D+T and n+<sup>4</sup>He pairs in relative motion with respect to each other<sup>16,17</sup>. This enables a fully integrated description of the reaction in the incoming (outgoing) channel, where the reactants (products) are far apart, as well as when all five nucleons are close together.

Arriving at a precise description of the DT fusion is not a simple task. In a previous work, for technical reasons we were not able to obtain results of comparable fidelity due to the omission of the 3N force<sup>18</sup>. Numerous studies have shown that this component of the nuclear interaction is essential for the reproduction of single-particle properties<sup>12,17-20</sup>, masses<sup>21-23</sup> and spin properties<sup>17,24</sup>, all impactful in the present case. Besides the addition of the 3N force, another crucial advance of the present versus our previous work lies in the accurate description of the 3/2<sup>+</sup> resonance as a correlated, localized system of five nucleons by means of the extension of the model space to include static <sup>5</sup>He eigenstates. The formation of this rather long-lived resonance as five-nucleon correlations built up during the fusion process is integral to the reaction mechanism, enhancing the computed cross section by an order of magnitude. Finally, the effect of the continuum of the D projectile, lying only at 2.224 MeV above the reaction threshold, is addressed with a discretization of the positive energy states of the two-nucleon system.

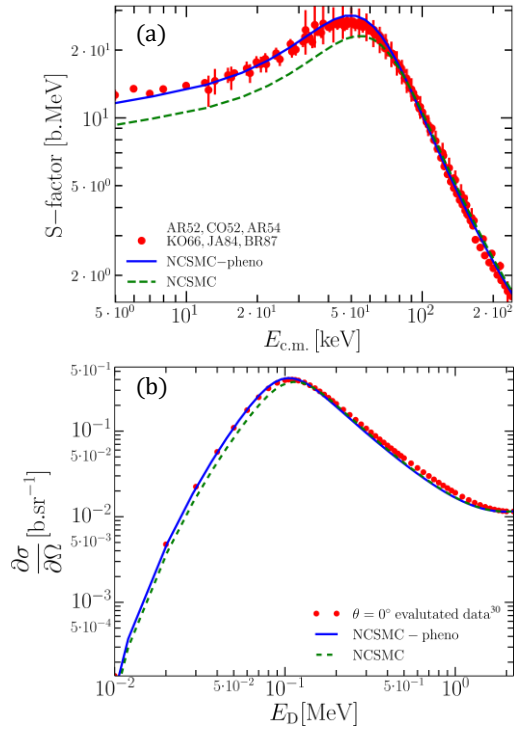


Figure 1: Astrophysical S-factor (a) and angular differential cross section at  $\theta_{c.m.} = 0^\circ$  (b) as a function of the energy in the c.m. frame. The result of the present calculations before (green dashed lines) and after (blue solid lines) phenomenological correction are compared with available nuclear data for the S-factor<sup>25-29</sup> and an evaluation of the differential cross section<sup>30</sup> (red circles).

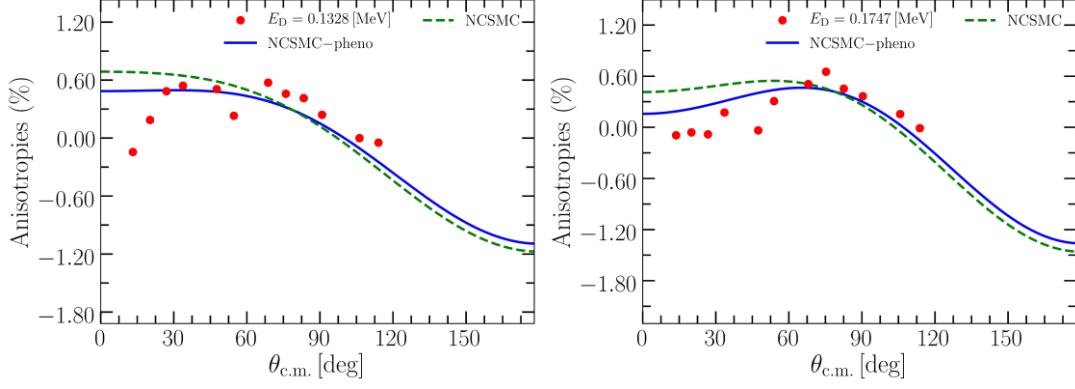


Figure 2: Computed (lines) and measured<sup>34</sup> (symbols) angular distribution (differential cross section relative to the total – angle-integrated – cross section) for the deuteron energies of 132.8 keV (left panel) and 174.7 keV (right panel). The effects of the correction to the position of the  $3/2^+$  resonance is shown (NCSMC, blue solid lines) with respect to the original NCSMC results (green dashed lines)

## Results

We begin our study with a validation of our *ab initio* reaction model on existing experimental data for the unpolarized DT reaction<sup>25-29</sup>. In Figure 1(a), we review the agreement of our computed astrophysical S-factor with established measurements. The S-factor isolates the nuclear dynamics by factoring out the Coulomb component of the total reaction cross section. The experimental peak at the c.m. energy of  $E_{c.m.} = 49.7$  keV corresponds to the enhancement from the  $3/2^+$  resonance of  $^5\text{He}$ . We underpredict by 15% the experiment (green dashed line versus red circles), an outcome that can be traced back to the overestimation of the  $3/2^+$  resonance centroid by a few keV, stemming from residual inaccuracies of the nuclear interaction<sup>17</sup>. To overcome this issue and arrive at an accurate evaluation of polarized DT reaction observables, we apply a phenomenological correction of  $-5$  keV to the position of the resonance centroid, achieving a remarkable agreement with the experimental S-factor over a wide range of energies (blue line). A detailed explanation of how such correction was obtained can be found in the Methods section. As a further validation of our calculations in Figure 1(b) we present the differential cross section in the center of mass frame at the scattering angle of  $\theta_{c.m.} = 0^\circ$  over a range of energies up to the deuterium breakup threshold. Our results (blue solid and green dashed lines) match the differential cross section of ref. 30 (red circles), obtained from a Legendre coefficient fit of measurements.

Having validated our calculation on precision measurements of unpolarized DT fusion, we now turn to the fusion of polarized DT fuel. The tritium has a spin of  $1/2$ , consequently its initial spin state is fully characterized by the Cartesian spin projection onto the axis of quantization (z axis),  $q_z$ . On the other hand, the deuterium is a spin-1 particle. Therefore, besides the equivalent  $p_z$  projection, an extra tensor value ( $p_{zz}$ ) is required to fully specify the spin state of the D beam. For the special case considered here, in which both reactants are aligned along the z axis, the polarized differential cross section assumes a fairly simple form and is given by,

$$\frac{\partial \sigma_{pol}}{\partial \Omega_{c.m.}}(\theta_{c.m.}) = \frac{\partial \sigma_{unpol}}{\partial \Omega_{c.m.}}(\theta_{c.m.}) \left( 1 + \frac{1}{2} p_{zz} A_{zz}^{(b)}(\theta_{c.m.}) + \frac{3}{2} p_z q_z C_{z,z}(\theta_{c.m.}) \right),$$

where  $A_{zz}^{(b)}$  and  $C_{z,z}$  are the beam tensor analyzing power and spin correlation coefficient, respectively. The general expression for arbitrary orientation of the spins is more complicated

and can be found in refs. 31-33. The main assumption used to estimate the 50% enhancement of the cross section for polarized DT fuel is that the reaction proceeds entirely through the  $J^\pi = 3/2^+$  partial wave with an orbital relative angular momentum of the D+T pair  $\ell = 0$  (i.e., in an  $s$ -wave of relative motion). Under such an assumption, the unpolarized differential cross section is isotropic (i.e., independent of the scattering angle). Furthermore, the integrals of  $A_{zz}^{(b)}$  and  $C_{z,z}$  over the scattering angle can be computed analytically and are 0 and  $1/3$ , respectively. This yields the estimate for the polarized reaction cross section  $\sigma_{pol} \approx \sigma_{unpol}(1 + \frac{1}{2}p_z q_z)$ , i.e. an enhancement factor of  $\delta = 1.5$  when  $p_z = q_z = 1$ .

The study of the anisotropy in the unpolarized differential cross section stands as a first stringent test of this estimate. When investigating the angular differential cross section divided by the reaction cross section (its integral over the scattering angle), as done before in the experiment of ref. 34, these appear as deviations from unity. As shown in Figure 2, a departure from a pure  $s$ -wave behavior is apparent. In particular,  $p$ -waves ( $\ell = 1$ ) are responsible for the oblique slope, and  $d$ -waves ( $\ell = 2$ ) for the making of a bump at  $90^\circ$ . Overall, we find good agreement with experiment once the centroid of the  $3/2^+$  resonance is correctly located. It is worth noting that the degree of anisotropy does not exceed the 1.6% level, leading to an absolute variation of the differential cross section of about 6.6 mb between  $0^\circ$  and  $180^\circ$ . The overall good reproduction of the data gives once again evidence of the high-quality of the computed collision matrix. Thereafter we present our *ab initio* results including the phenomenological adjustment of the  $3/2^+$  resonance centroid, and comment when appropriate, on its effect.

As a further test, we computed  $A_{zz}^{(b)}$  and  $C_{z,z}$  from the components of the S-matrix using the formalism of the density matrix. As benchmark, we verified that (under the condition of an unpolarized target) we could reproduce the beam analyzing powers derived and computed independently. In principle both these observables can be measured in a laboratory by analyzing the differences with respect to the unpolarized cross section when the deuteron beam is vector- and tensor-polarized, the tritium is vector-polarized, and beam and target polarizations are aligned along the  $z$ -axis. In practice, however, only the tensor analyzing power at  $\theta_{c.m.} = 0^\circ$  has been measured in the energy region relevant for thermonuclear fusion ( $0.24_{+0.18}^{-0.9}$  MeV)<sup>35</sup>. Our computed result ( $-0.975$ ) agrees well with experiment ( $-0.929 \pm 0.014$ ). The only available experimental data to test the angular distribution of the differential cross section, and hence the contribution of partial waves other than the  $J^\pi = 3/2^+, \ell = 0$  component at the relevant energies are measurements of the mirror  $D^3\text{He}$  fusion process. Such contribution of additional partial waves is exemplified in Figure 3(a), where we compare theoretical and experimental results for the  $D^3\text{He}$  tensor analyzing power at the deuteron incident energy of

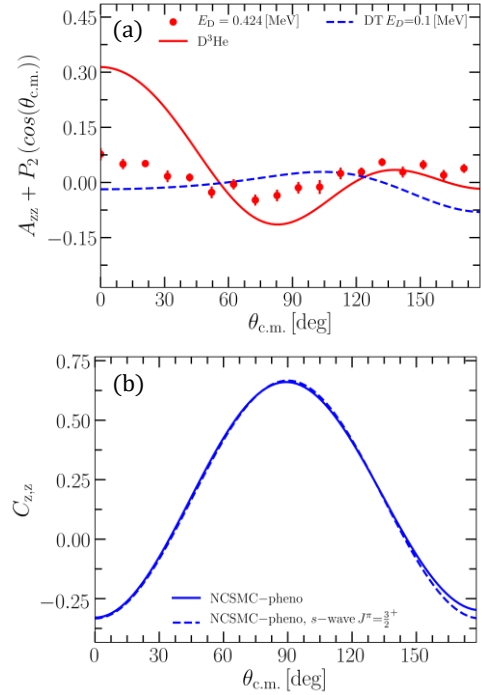


Figure 3: (a) Computed tensor analyzing power of the  $D^3\text{He}$  fusion reaction (red solid line) and data from ref. 36 (red circles) at the D incident energy  $E_D = 424$  keV compared to the prediction for the DT fusion reaction (blue dashed line) at the corresponding energy of  $E_D = 100$  keV. The  $s$ -wave contribution to the tensor analyzing power has been subtracted. (b) Computed spin correlation coefficient for the DT fusion at  $E_D = 128$  keV (solid blue line). The result obtained by disregarding the contribution of partial waves beyond the  $J^\pi = 3/2^+, \ell = 0$  (blue dashed line) is also shown for comparison. All calculations include the phenomenological correction.

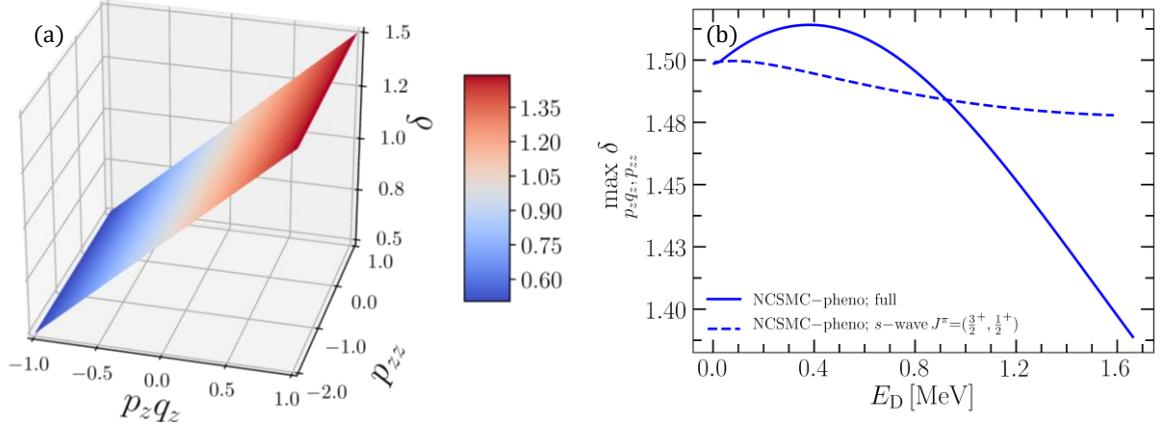


Figure 4: (a) *Ab initio* prediction of the enhancement factor of the polarized DT reaction cross section at  $E_d = 100$  keV as a function of the vector  $(p_z q_z)$  and  $(p_{zz})$  tensor polarization of the deuterium and tritium. (b) Computed maximum enhancement factor (over all possible values of  $p_z q_z$  and  $p_{zz}$ ) of the polarized DT cross section as a function of the deuteron incident energy  $E_D$  (solid line). The maximum enhancement is always found for  $p_z q_z, p_{zz} = 1$ . Due to the energy scale of the figure, the enhancement factor obtained without the phenomenological correction (i.e., the NCSMC result) is indistinguishable from the NCSMC-pheno curve. Also shown as a dashed line is the maximum enhancement factor obtained by retaining only the  $\ell = 0, J^\pi = 3/2^+$  and  $1/2^+$  partial waves. See the text for additional information.

0.424 MeV after subtraction of the  $s$ -wave contribution, which is simply given by the Legendre polynomial  $P_2(\cos \theta_{c.m.})$ . Our results are in fair agreement with the experimental data<sup>36</sup>, particularly for what concerns the shape of the distribution. At the same time, we find notable differences with respect to the predicted DT  $A_{ZZ}^{(b)}$  at the corresponding energy of  $E_D = 0.1$  MeV (where we take into account the difference in  $Q$ -values), highlighting a somewhat different partial-wave content in the two mirror reactions. This indicates that some caution has to be taken when using  $D^3He$  as a proxy for the study of polarization in the DT fusion process. All in all, Figure 3(a) gives added confidence in the polarization observables predicted for the DT fusion. More details on the calculation of the  $D^3He$  reaction observables can be found in the Supplemental Information.

The differential cross section for all angles is required for the computation of the polarized reaction cross section  $\sigma_{pol}$  and the enhancement factor  $\delta$ , which we obtain (for any initial spin configuration) as the ratio of the latter to  $\sigma_{unpol}$ . As shown in Figure 4(a), at the deuteron incident energy of 100 keV the *ab initio* calculation recovers and confirms the ideal enhancement factor for  $p_z, q_z = 1.0$ , which is a result independent of the model space size and the phenomenological correction. Indeed, while our *ab initio* calculations show that the reaction is not exactly isotropic, at this energy the deviations of  $A_{ZZ}^{(b)}$  and  $C_{z,z}$  from a pure  $J^\pi = 3/2^+, \ell = 0$  contribution are substantial only in the proximity of  $\theta_{c.m.} = 180^\circ$  [see, e.g., Figure 3(b)], and hence have only a minor effect on angle-averaged observables, such as the reaction cross section. We note that  $\delta$  is nearly independent of the value of  $p_{zz}$ , indicating that the analyzing power of the deuterium does not play any role in the enhancement of the cross section (a consequence of the nearly-zero value of the integral of  $A_{ZZ}^{(b)}$ ). However, the factor  $\delta$  varies as a function of the energy and drops significantly above the deuteron incident energy of 0.8 MeV. This is shown in Figure 4(b) for the maximum enhancement (which is found for  $p_z q_z, p_{zz} = 1$ ). Interestingly, the peak value of the maximum enhancement (located around  $E_D = 0.4$  MeV) is somewhat larger than the estimated 1.5 value. This is mainly an effect of  $3/2^+, \ell = 2$  contributions. For comparison we also show the maximum enhancement obtained when we only include the  $J^\pi = 3/2^+,$  and  $1/2^+$  partial waves with an orbital relative angular momentum

of the D+T pair of  $\ell = 0$ . This shows the influence of  $1/2^+$  components of the wave function below and above the  $3/2^+$  resonance even in a purely s-wave picture of the reaction. When also the  $1/2^+$  partial wave is removed, we recover the (energy independent) 1.5 estimate.

In Figure 5 we show the polarized fusion reaction rate for typical values of vector and tensor polarization of the deuterium ( $p_z, p_{zz}$ ) and tritium ( $q_z$ ) that can be readily obtained in the laboratory, that is  $p_z, p_{zz} = 0.8$  and  $q_z = \pm 0.8$ , respectively. This quantity, obtained from averaging the reaction cross section over the distribution of the reactants' speeds (assumed to be Maxwellian)<sup>37</sup>,

$$\langle \sigma v \rangle = \sqrt{\frac{8}{\pi \mu (k_b T)^3}} \int_0^\infty S(E) \exp\left(-\frac{E}{k_b T} - \sqrt{\frac{E_g}{E}}\right) dE,$$

is a measure of how rapidly the reaction occurs and is an important input in astrophysics and plasma simulations. The constant  $\mu$  is the reduced mass of the reacting nuclei (D and T),  $k_b$  and  $T$  are respectively the Boltzmann constant and the temperature,  $S(E)$  stands for the (computed) S-factor and  $E_g$  is the Gamow energy given by  $2\mu(\pi e^2)^2/\hbar^2$ . In the figure we also compare our unpolarized reaction rate to those obtained from the parameterization of DT fusion data of Bosch and Hale<sup>38</sup>, the phenomenological  $R$ -matrix fit of Descouvemont et al.<sup>39</sup>, and the potential model calculation adopted in the NACRE compilation<sup>40</sup>, which is intended for applications in astrophysics simulations. Overall, we find that they agree well even at energies above the resonance. In more detail, our calculation agrees best with the phenomenological  $R$ -matrix evaluation, particularly at higher energies where data are typically scarcer. In our case, the uncertainties due to the finiteness of the model space are indistinguishable from the line width. The convergence of our *ab initio* model is discussed in the Supplemental Information. A further analysis of the systematic and statistical uncertainties associated with the adopted nuclear interaction model, such as those stemming from the order of the chiral expansion or the uncertainty in constraining its parameters, is presently computationally prohibitive. The phenomenological correction induces a global shift towards the reaction threshold, commensurate with that of the resonance centroid. In practice, this fine tuning is tightly constrained by the requirement to match S-factor data in the energy range below the resonant peak. The *polarized* reaction rate shows the same shape, albeit globally enhanced by a factor of  $\sim 1.32$ , in agreement with the approximate estimate for the chosen polarization values. This result follows from the rather slow variation of the enhancement factor of the reaction cross section as a function of the energy in the narrow Gamow window (deuteron incident energies below a few hundred keV) where the product of the Maxwell-Boltzmann distribution with the tunneling probability of the nuclei through their Coulomb barrier is significantly different from zero. It is interesting to note that with polarization a reaction rate of equivalent magnitude as the apex of the unpolarized reaction rate is reached at lower

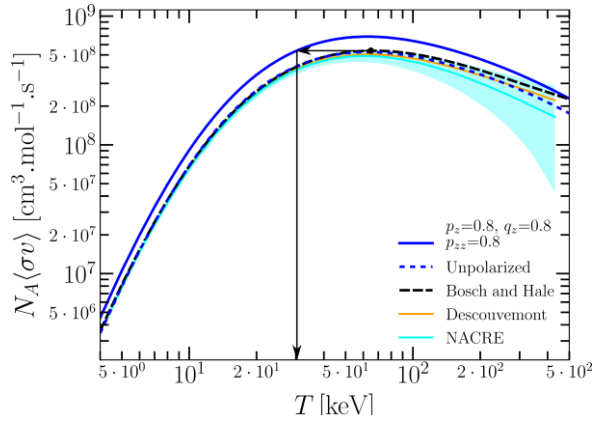


Figure 5: Comparison between the computed (NCSMC-pheno) DT reaction rate for unpolarized (blue dashed line) and polarized fuel with aligned spins (blue solid line). We use reactant polarization parameters achievable in the laboratory. Also shown for comparison are the unpolarized reaction rates obtained from the widely adopted parametrization of the DT fusion cross section of Bosch and Hale<sup>38</sup> (black long-dash line), from the  $R$ -matrix fit of Descouvemont<sup>39</sup> (yellow line) and from the NACRE compilation<sup>40</sup> (cyan line and band).

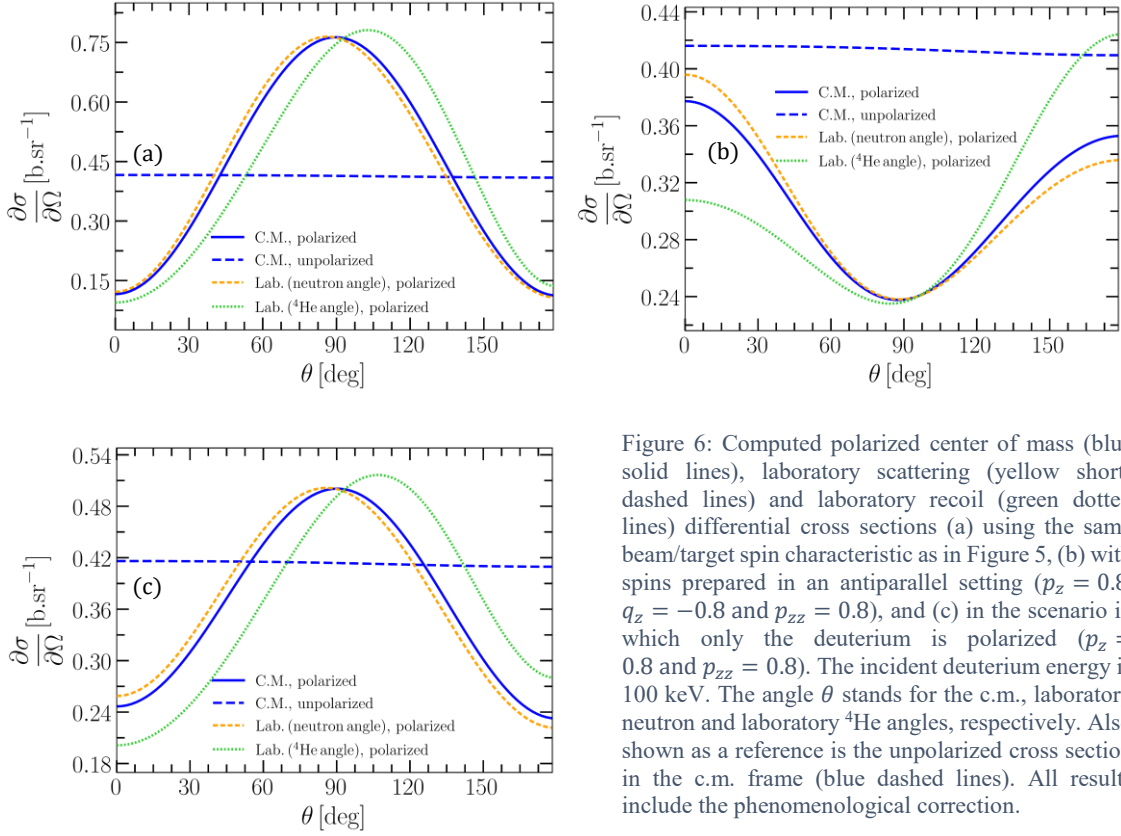


Figure 6: Computed polarized center of mass (blue solid lines), laboratory scattering (yellow short-dashed lines) and laboratory recoil (green dotted lines) differential cross sections (a) using the same beam/target spin characteristic as in Figure 5, (b) with spins prepared in an antiparallel setting ( $p_z = 0.8$ ,  $q_z = -0.8$  and  $p_{zz} = 0.8$ ), and (c) in the scenario in which only the deuterium is polarized ( $p_z = 0.8$  and  $p_{zz} = 0.8$ ). The incident deuterium energy is 100 keV. The angle  $\theta$  stands for the c.m., laboratory neutron and laboratory  $^4\text{He}$  angles, respectively. Also shown as a reference is the unpolarized cross section in the c.m. frame (blue dashed lines). All results include the phenomenological correction.

temperatures, i.e. less than 30 keV compared to 65 keV (where both rates peak), as highlighted in Figure 5 by the arrows. As a naive illustration, this means that by using polarized DT fuel the output of a standard fusion reactor could either be enhanced by 32% or its operational temperature decreased by as much as 45%. A more comprehensive discussion of the economics of using *polarized* fuel in the case of inertial confinement fusion can be found in ref. 4.

While the deviations from a pure  $J^\pi = 3/2^+, \ell = 0$  contribution are small and have only a minor effect in particular on angle-averaged observables such as the reaction cross section or the reaction rate, they play a somewhat larger role on the angular distribution of the reaction products, especially when the reactants' spins are not in a parallel setting. In particular, while the tensor analyzing power  $A_{zz}^{(b)}$  has virtually no impact on the enhancement factor, it is the main driver of the shape of the angular distribution of the polarized cross section, shown in Figure 6. To better visualize the situation in the laboratory, in addition to the differential cross section in the c.m. frame we also plot the differential cross section in the laboratory frame as a function of the laboratory neutron and  $\alpha$ -particle angles in yellow short-dashed and green dotted lines, respectively. The anisotropy of the angular differential cross section is highly sought after because it can be used to force the emitted neutrons and  $\alpha$  to be two to five times more focused towards the reactor blanket [Figure 6(a) and 6(c)], which collects the energy released, than along the polarization axis, or twice the exact opposite [see Figure 6(b)]. That is, the reaction products are more focused along the magnetic field. The former conditions can be achieved using only polarized deuterium or fully polarized DT fuel. The latter is obtained in the situation where the D and T spins are anti-aligned, leading to a reduction of the cross section of up to a factor of 0.5, as illustrated in Figure 4(a).

## Conclusion

We have performed *ab initio* no-core shell model with continuum calculations with modern chiral EFT nucleon-nucleon and three-nucleon interactions for the DT fusion and its mirror  $D^3\text{He}$  reaction. We were able to reproduce the cross sections of these reactions with unpolarized reactants. Our calculations discriminate among DT reaction rates from phenomenological evaluations and demonstrate in detail the small contribution of  $\ell > 0$  partial waves in the vicinity of the  $3/2^+$  resonance. We predict the DT reaction rate for realistically polarized reactants ( $p_z, q_z \sim 0.8$ ) and show that the reaction rate increases by about 32% compared to the unpolarized one and, further, the same reaction rate as the unpolarized one can be achieved at ~45% lower temperature. These results also endorse the application of the present approach to the evaluation of the polarized DD fusion, where the non-resonant character of the reaction prevents even a simple estimate of the enhancement factor in the ideal scenario of perfect spin-alignment of the reactants.

## Methods

### No-Core Shell Model with Continuum

Our approach to the description of the DT fusion reaction is the *ab initio* no-core shell model with continuum (NCSMC) introduced in ref. 14 and applied to nucleon<sup>12,19,20</sup>, deuterium<sup>13</sup>, tritium and <sup>3</sup>He induced reactions<sup>41</sup> and the three-cluster continuum dynamics of the Borromean <sup>6</sup>He nucleus<sup>42</sup>. Presently, it is the only *ab initio* reaction method capable to efficiently describe complex light-nuclei reactions and in particular transfer reactions, though a complementary approach based on lattice effective field theory offers a more efficient avenue to the calculation of scattering and reactions induced by  $\alpha$  particles<sup>43</sup>.

The approach starts from the wave functions of each of the colliding nuclei and of the aggregate system, obtained within the *ab initio* no-core shell model (NCSM)<sup>15</sup> by working in a many-body harmonic oscillator (HO) basis. This is a configuration interaction method in which all nucleons are treated as active degrees of freedom and the model space includes all possible excitations of the system up to a maximum of  $N_{\text{max}}$  quanta above the minimum-energy configuration. It then uses the NCSM static solutions for the aggregate system and continuous ‘microscopic-cluster’ states, made of pairs of nuclei in relative motion with respect to each other, as an over-complete basis to describe the full dynamical solution of the system. That is, the ansatz for the five-nucleon ( $A = 5$ ) wave function takes the form of a generalized cluster expansion (here specifically shown for the present case of a <sup>5</sup>He aggregate system):

$$|\Psi^{J\pi I}\rangle = \sum_{\lambda} c_{\lambda}^{J\pi I} |{}^5\text{He}; \lambda J^{\pi I}\rangle + \sum_{\nu} \int dr r^2 \frac{\gamma_{\nu}^{J\pi I}(r)}{r} \hat{A}_{\nu} |\Phi_{\nu r}^{J\pi I}\rangle,$$

where  $J, \pi$  and  $I$  denote respectively total angular momentum, parity and isospin quantum numbers. The first term on the right-hand side of the equation is an expansion over the discrete energy-eigenstates of the <sup>5</sup>He nucleus (indexed by  $\lambda$ ) obtained within the NCSM method to incorporate the physics of the five nucleons in close contact. The second term is tailored to tackle the scattering and long-range clustering of the system. The index  $\nu = \{\nu_{\text{TD}}, \nu_{\text{an}}\}$  runs over the reaction channels, defined by the mass partition (D+T and n+<sup>4</sup>He, respectively) and the quantum numbers characterizing the reacting bodies and their relative motion. The continuum basis states  $\Phi_{\nu r}^{J\pi I}$  are antisymmetrized by the operator  $\hat{A}_{\nu}$ , and, in the case of the present binary collision, read:

$$|\Phi_{\nu_{\text{TD}} r}^{J\pi I}\rangle = [ [|{}^3\text{H}; \lambda_{\text{T}} J_{\text{T}}^{\pi_{\text{T}}} I_{\text{T}}\rangle |{}^2\text{H}; \lambda_{\text{D}} J_{\text{D}}^{\pi_{\text{D}}} I_{\text{D}}\rangle ]^{S_{\text{DT}} I} Y_{\ell_{\text{TD}}}(\hat{r}_{\text{TD}})]^{J\pi I} \frac{\delta(r - r_{\text{TD}})}{r r_{\text{TD}}},$$

and

$$|\Phi_{\nu_{\text{an}} r}^{J\pi I}\rangle = [ [|{}^4\text{He}; \lambda_{\alpha} J_{\alpha}^{\pi_{\alpha}} I_{\alpha}\rangle |n\rangle ]^{S_{\text{an}} I} Y_{\ell_{\text{an}}}(\hat{r}_{\text{an}})]^{J\pi I} \frac{\delta(r - r_{\text{an}})}{r r_{\text{an}}}.$$

The first set of continuum states describes the incoming T and D nuclei in relative motion, with  $\vec{r}_{\text{TD}}$  the separation between their centers of mass, while the second set represents the outgoing wave of relative motion between the ejected  $\alpha$  and neutron particles with separation  $\vec{r}_{\text{an}}$ . (Expressions in squared brackets denote angular momentum coupling.) The discrete coefficients  $c_{\lambda}^{J\pi I}$  and continuous amplitudes of relative motion  $\gamma_{\nu}^{J\pi I}(r)$  are obtained by solving

the generalized eigenvalue problem derived from representing the non-relativistic Bloch-Schrödinger equation in the model space spanned by the discrete and continuum basis states of the NCSMC. The scattering matrix – and from it all reaction observables – are finally obtained by matching these solutions with the known asymptotic behavior of the wave function at  $r = 18$  fm, using the coupled-channel  $R$ -matrix method on a Lagrange mesh<sup>44,45</sup>.

### Details of the calculation

We start from a five-nucleon Hamiltonian including NN<sup>9</sup> and 3N<sup>10-13</sup> interactions at the fourth and third order of chiral EFT, respectively, with a 500 MeV cutoff. This interaction is then softened by the means of the similarity renormalization group (SRG) technique to a resolution scale of  $\Lambda_{\text{SRG}} = 1.7 \text{ fm}^{-1}$ , enabling good convergence properties within the currently largest HO basis size achievable. The computational challenges of the present work limited such a basis size to a maximum number of HO excitations of  $N_{\text{max}} = 11$ . For the HO frequency, we chose the value of  $\hbar\omega = 16$  MeV, which was found to speed up the convergence rate with respect to  $N_{\text{max}}$ .

Besides the size of the HO model space, the convergence properties of the present calculations are also affected by the number of discrete eigenstates of the  $A=2$ -, 3-, 4- and 5-nucleon systems used to construct the NCSMC trial wave function. We included the first fourteen discrete energy-eigenstates of the <sup>5</sup>He system (two  $J^\pi = 1/2^-$ , three  $3/2^-$ ,  $5/2^-$ ,  $7/2^-$ , three  $1/2^+$ , two  $3/2^+$ ,  $5/2^+$ ,  $7/2^+$ ), the ground state and up to 8 positive-energy eigenstates (5 in the <sup>3</sup> $S_1$ -<sup>3</sup> $D_1$  and 3 in the <sup>3</sup> $D_2$  channels) of the deuterium, and the ground states of the <sup>3</sup>H and <sup>4</sup>He nuclei. The close vicinity of the energy continuum of the deuterium, only bound by 2.224 MeV, leads to distortion effects the description of which necessitates the inclusion of positive-energy eigenstates<sup>18,13</sup>. Analogous distortion effects are less pronounced in the more bound triton and  $\alpha$  particles, and are efficiently addressed indirectly through the inclusion of the eigenstates of the aggregate <sup>5</sup>He system<sup>12,17</sup>.

A particular challenge in the presence of 3N forces is the dependence on the parameter  $E_{3\text{max}}$ . This embodies the size of the three-nucleon single-particle HO basis used to represent the 3N interaction. For technical reasons, the largest  $E_{3\text{max}}$  value computationally achievable is currently of 17 HO quanta. High energy 3N force components of the NCSMC Hamiltonian can be slowly converging as a function of this parameter. Since they represent a small perturbation with respect to the NN contribution, we omit them for basis states at the boundary of the model space.

### Phenomenological correction

Remaining inaccuracies in the adopted chiral Hamiltonian prevent an accurate (of the order of less than a few keV) reproduction of the sub  $p$ -shell levels. This was already observed for the <sup>5</sup>He system in ref. 17 particularly in Figure 16, which illustrates the residual imprecisions for the reproduction of  $p$ -shell spectroscopy. It is then not surprising that the DT fusion S-factor is not perfectly reproduced (see Figure 1). To address this difficulty, we treated the eigenvalue of the second  $3/2^+$  NCSM energy-eigenstate (one of the static basis states that serve as input to represent our solution) as an adjustable parameter and constrained it to the value that yielded the best fit of the experimental S-factor data for energy below the resonance. In practice, this resulted in a shift of  $-86$  keV of the  $N_{\text{max}} = 11$  <sup>5</sup>He  $3/2^+$  eigenenergy computed within the NCSM, which was initially  $-8.186$  MeV, while the microscopic  $n+^4\text{He}$  and  $\text{D}+\text{T}$  cluster potentials and all other characteristics of the scattering matrix continued to be predicted within

the *ab initio* method. The amplitude of the correction is less substantial than it appears. In the NCSMC Hamiltonian, the coupling matrix elements between the aggregate system and microscopic-cluster states are given by the NCSM eigenvalues multiplied by the cluster form factor (the overlap between the two type of basis states). As a consequence, the effect of this adjustment is a considerably smaller shift of  $-5$  keV of the resonance centroid  $E_r$  extracted from the  $3/2^+$  eigen-phaseshifts computed within the NCSMC, shown in Table 1 of the Supplemental Information. Because the  $3/2^+$  resonance is close to the D+T threshold, the S-factor is very sensitive to its centroid. Assuming a Breit-Wigner formula for the reaction cross section one can estimate the S-factor to be proportional to  $1/E_r^2$  close to threshold and to follow a  $1/E_{\text{c.m.}}^2$  slope after the resonance. This explains our results, and why our phenomenological adjustment is tightly constrained by reproducing the S-factor close to threshold. We refer to the modified calculation as NCSMC-pheno.

## Supplemental Information

### Convergence of the calculation

Achieving convergence with respect to the number of eigenstates of the aggregate  ${}^5\text{He}$  system is straightforward. All eigenstates in a large range of energies around the region of interest for the DT fusion can be effortlessly included. The second  $3/2^+$  eigenstate is exceptionally impactful. This can be clearly seen in Figure 7 by comparing the S-factor (dominated by the  $3/2^+$  component of the wave function) computed within the full NCSMC model space with the results obtained within the cluster basis alone. Evidently, the configuration where all five nucleons are in close contact plays an essential role.

Figure 7 also shows the somewhat slow but steady convergence pattern of the S-factor with respect to the number (in order of increasing energy) of positive-energy eigenstates of the D projectile included in addition to the (negative-energy) ground state. We used the notation  $d$  and  $d^*$  for the eigenstates in the  ${}^3S_1$ - ${}^3D_1$  and  ${}^3D_2$  channels of  ${}^2\text{H}$ , respectively. Since the number of available positive-energy eigenstates of the D projectile depends on the HO basis size (higher  $N_{\text{max}}$  means more states to discretize the  ${}^2\text{H}$  continuum), it is instructive to compare this figure with the convergence in  $N_{\text{max}}$  (Figure 8). The agreement between the  $N_{\text{max}} = 9$  and 11 calculations (both including the maximum number of available deuteron states) is quite good.

It should be noted that the S-factor is extremely sensitive to changes in the position of the  $3/2^+$  resonance, acting as a magnifying glass. For example, the 35 keV shift to lower energies in the resonance position between the results obtained within the cluster basis alone and the full NCMC model space (see Table 1) results in about one order of magnitude increase of the S-factor amplitude. In comparison, the positive-energy eigenstates of the D projectile contribute a shift of 10 keV (15 keV) in the  $3/2^+$  resonance centroid when the eigenstates of the aggregate  ${}^5\text{He}$  system are (are not) included in the model space. This suggests that there is a strong similarity between some cluster basis states built from the discretization of the D energy continuum and some static solutions of the  ${}^5\text{He}$  aggregate. In this contest, it becomes also clear that the fine-tuning of the  $3/2^+$  resonance centroid required to accurately reproduce the experimental S-factor is extremely challenging, given remaining inaccuracies of the adopted chiral interactions for  $p$ -shell nuclei. For this reason, we opted for a phenomenological fine tuning as it will be explained in the next section.

The  $3/2^+$  resonance, which drives the massive enhancement of the S-factor, schematically consists in a proton promoted from the  $s$ -shell onto the  ${}^2p_{3/2}$  sub-shell, as shown in the sketch of Figure 9. The energy required is of the order of the splitting between major HO  $s$ - and  $p$ -shells and can be inferred from the experimental spectra as approximately the excitation energy of the  $3/2^+$  resonance, that is 16.84 MeV. This explains why the HO frequency of 16 MeV chosen in this work contributes to speeding up the convergence of our calculations. Additionally, in order to ensure the convergence of our calculation within the computationally achievable largest model space ( $N_{\text{max}} = 11$ ), we used an SRG resolution scale of  $\Lambda_{\text{SRG}} = 1.7 \text{ fm}^{-1}$ . To further analyze our parameters' choice, in Figure 10 we compare the present  $n + {}^4\text{He}$  elastic scattering phase shifts (obtained in the NCSMC model space without D+T cluster states) with those previously obtained for  $\hbar\omega = 20 \text{ MeV}$ ,  $\Lambda_{\text{SRG}} = 2.0 \text{ fm}^{-1}$  and  $N_{\text{max}} = 13$ <sup>17,47</sup>. We can see that the agreement is excellent. The fast convergence rate achieved within the present choice of parameters is even more manifest when analyzing the dependence on  $N_{\text{max}}$  of

the  ${}^5\text{He } 3/2^+$  eigenenergy computed within the NCSM. This is illustrated in Table 2, where we show the difference between the computed eigenenergy at a given  $N_{\text{max}}$  relative to the extrapolated energy at  $N_{\text{max}} \rightarrow \infty$ . The frequency closer to the major HO shell splitting performs much better. At  $N_{\text{max}} = 11$  the relative difference goes down from 25.68% at  $\hbar\omega = 20$  MeV,  $\Lambda_{\text{SRG}} = 2.0 \text{ fm}^{-1}$  to 8.41% at  $\hbar\omega = 16$  MeV,  $\Lambda_{\text{SRG}} = 1.7 \text{ fm}^{-1}$ , more than a factor of two.

## Reaction Mechanism

The centroid and width of the  $3/2^+$  resonance computed within the NCSMC-pheno are in good agreement with those extracted from the  $R$ -matrix analysis of data of ref. 48, particularly considering that the latter values were obtained from the  $S$ -matrix pole rather than from the eigenphaseshift, as done here. In addition, the magnitude and width of the computed total  $n$ - ${}^4\text{He}$  cross section in the energy region of the  $3/2^+$  resonance are in a good agreement with the measurements of Haesner et al.<sup>49</sup>, though the position of its peak is overestimated by about 1%. This is due to remaining inaccuracies of the adopted chiral interactions for  $p$ -shell nuclei which cannot be entirely corrected using the minimal (single-parameter) phenomenological adjustment adopted in this work. In Figure 11, we show the (real part of the) phase shifts extracted from the diagonal elements of the  $S$ -matrix in the  $J = 3/2^+$  channel, namely the  $d$ - ${}^3\text{H}$   ${}^4S_{3/2}$  and  $n$ - ${}^4\text{He}$   ${}^2D_{3/2}$  partial waves belonging, respectively, to the entrance and exit channels of the reaction. Similar to our more limited work of ref. 18, we find a sharp resonant behavior in the  $d$ - ${}^3\text{H}$   ${}^4S_{3/2}$  partial wave, but the  $n$ - ${}^4\text{He}$   ${}^2D_{3/2}$  phase shift is broader and does not cross  $90^\circ$ . Figure 11 also highlights the influence of the deuterium continuum. We would like to stress that this reaction mechanism highlights the fundamental role played by the tensor force, present in both NN and 3N components of the nuclear interactions. In addition, the important role of the 3N force in reproducing the position of the resonance centroids and the splitting of the  ${}^2p_{3/2}$  and  ${}^2p_{1/2}$  sub  $p$ -shell levels has also become evident in the last decade<sup>47,50</sup>. Because of this (and the fact that the SRG procedure we use to accelerate the convergence generates induced 3N forces) the inclusion of 3N forces was essential to achieving the present accurate results for the DT fusion.

## Comparison to higher energy data

As discussed, our approach is presently valid up to the threshold of the dissociation of the deuterium projectile or 2.224 MeV. Above such energy, it represents an approximation. Nevertheless, in Figure 12 and 13 we present a comparison with higher-energy data for the angular differential cross section and tensor analyzing power, respectively. At the deuteron energy of 2.2 MeV and above, the *ab initio* angular differential cross section systematically underestimates the data<sup>29,51-54</sup>, though the shape of the angular distribution is qualitatively reproduced. The tensor analyzing power (presented in Figure 13), which is inversely proportional to the differential cross section, further magnifies the difference between theory and experiment. At the origin of this discrepancy are higher-energy  ${}^5\text{He}$  resonances (known experimentally and in evaluations<sup>55</sup>) that come into play a few MeV above the peak-energy of the DT fusion, due to the population of the nearby  ${}^2p_{1/2}$  subshell (see the sketch of Figure 9). Lacking an exact treatment of three-cluster dynamics and given remaining inaccuracies of the adopted chiral Hamiltonian in reproducing the  $p$ -subshell ordering that affects the underlying phase shifts, these resonances are not reproduced with the required level of accuracy (within  $\sim 10$  keV). We note that this only affects the cross section at higher energies. In particular,

around the energy of interest for fusion applications ( $\sim 100$  keV), the tensor analyzing power is in good agreement with experiment.

### Calculation for the mirror $D^3\text{He}$ reaction

In Figure 14, we compare our computed  $D^3\text{He}$  S-factor and its phenomenological correction to available data<sup>36,56-62</sup>. All parameters of the NCSMC calculation match those of Figure 1 but the  $N_{\text{max}}$  value, which in this case is limited to nine major shells for computational reasons. As in the DT case, the centroid position of the  $3/2^+$  resonance of  $^5\text{Li}$  is overestimated and needs to be corrected phenomenologically. Once again, the adjustment of the  $3/2^+$  resonance is strongly constrained by reproducing the S-factor from  $\sim 20$  keV to energies below the resonance. At lower energies (below  $\sim 20$  keV), the prediction is expected to be in disagreement with data due to laboratory electron screening effects, which enhance the cross section masking the (“bare”) nuclear S-factor. At the peak of the S-factor, the experimental picture is somewhat uncertain. Our results are in good agreement with the data of ref. 60 (CO05). The computed peak value of the reaction cross section (798 mb) is in good agreement with the experimental value of  $777 \pm 33$  mb reported by Geist et al. (GE99)<sup>36</sup>. However, the position of the peak is found at 450 keV, 24 keV above the energy reported in ref. 36. This slight energy shift is at the origin of the discrepancy between our calculation and the S-factor of Geist et al. In the present (restricted)  $N_{\text{max}} = 9$  model space, a 426 keV peak energy is inconsistent with the behavior of the S-factor at lower energy. There, we find good agreement with the total reaction cross section and thermalized cross section data of refs. 63-64 and 61, respectively, owing to the tight constraint imposed by this energy regime on our phenomenological adjustment [see Figure 15(a) and 15(b)]. In Figure 15(c) we compare the computed differential cross section at  $\theta_{\text{c.m.}} = 90^\circ$  with the experimental data up to  $E_D = 1.6$  MeV of Klucharev et al.<sup>65</sup>. Overall, a small overestimation of data is noticeable above the fusion peak suggesting once again that the width of the  $3/2^+$  resonance may be slightly overestimated. Based on the trend shown by the DT results of Figure 8, we expect that an  $N_{\text{max}} = 11$  calculation would yield a narrower cross section peak in closer agreement with the experimental data of both Geist et al and Klucharev et al. We also computed an array of polarization observables, namely the vector  $A_y^{(b)}$  and tensor  $A_{zz}^{(b)}$ ,  $A_{yy}^{(b)}$ , and  $A_{xz}^{(b)}$  analyzing powers at the deuteron incident energies of 99, 424 and 641 keV, and the polarization transfer coefficient  $K_y^{y'}$  at  $\theta_{\text{c.m.}} = 0^\circ$ , to compare to the measurements reported in refs. 36 and 66, respectively. The comparisons for the analyzing powers are shown in Figures 3(a), 15(d), and 16(a)-(c), while that for the polarization transfer coefficient is presented in Figure 16(d). In general, we find fairly good agreement with the experimental data at 424 keV, while at the left and right of the peak we tend to obtain a good description of the overall angular and energy dependence but somewhat overestimate the amplitude. This can be traced back to the modest overestimation of the reaction cross section. Finally, in Figure 17 we compare our computed spin correlation coefficients  $C_{1,1,1,-1}$ ,  $C_{1,0,1,1}$  and  $C_{1,1,1,1}$  to the experimental data of ref. 6, at the incident deuteron energy of 430 keV. This is the only existing spin-correlation experiment in the resonance region for this reaction, and the most significant and direct test of our calculations for the polarized fusion. In our notation, the coefficients are written as spherical tensors with the initial (final) two indices corresponding to the rank and projection of the tensor moments of the beam (target). Our calculation agrees well with the experimental data. This stands as a chief validation of our predictions for the polarized DT fusion. Overall, our *ab initio* method together with modern chiral NN+3N interactions are able to reproduce both the DT fusion and its mirror

D<sup>3</sup>He reaction. This is a major step forward compared to the results obtained in our earlier work<sup>18</sup>.

### Discussion of uncertainties

In the present work, uncertainties derive either from the many-body model used to solve the five-body Schrödinger equation or from the employed nuclear Hamiltonian. The former are addressed in the section concerned with the convergence of the NCSMC method. There, we show that our calculation is converged with respect to the three parameters  $\hbar\omega$ ,  $N_{\max}$  and  $\Lambda_{\text{SRG}}$ . Thus, uncertainties from the many-body technique are particularly small, typically close to the size of the line width as exemplified in Figure 6. To demonstrate that the accuracy of the present application is not accidental, we computed the D<sup>3</sup>He mirror reaction and compared both unpolarized and polarized reaction observables to data. We obtained satisfactory agreement with data that further validates our predictions for the DT polarized observables. On the other hand, it is computationally extremely challenging for the time being to give an estimate of the uncertainties pertaining the nuclear Hamiltonian. We use a chiral EFT Hamiltonian that has been proven to reproduce properties of the  $A = 3, 4, 5, 6$  nuclei, including  $p$ -shell physics. Based on the fact that other chiral EFT Hamiltonians have emerged that fail to reproduce the low-lying  $p$ -waves of the <sup>5</sup>He system, it is expected that uncertainties from the nuclear interaction model may be significant, but this remains to be investigated.

Supplemental Information: Figures and Tables

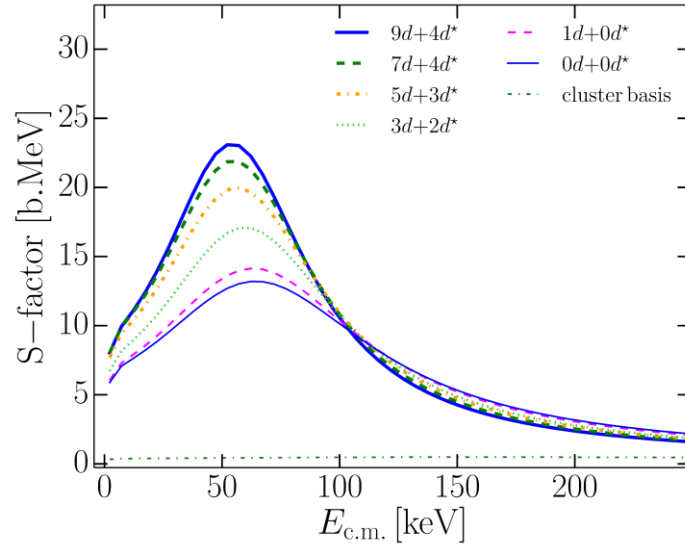


Figure 7: Convergence of DT S-factor as a function of the number of positive-energy eigenstates of the deuterium projectile as obtained within the NCSMC approach at  $N_{\max} = 11$ . We used the notation  $d$  and  $d^*$  for the eigenstates in the  ${}^3S_1$ - ${}^3D_1$  and  ${}^3D_2$  channels of  ${}^2\text{H}$ , respectively. Results obtained within the cluster basis alone (with the deuterium ground state only) are shown as reference (green dash-dotted line).

${}^5\text{He}(3/2^+)$	Cluster basis (D g.s. only)	Cluster basis	NCSMC (D g.s. only)	NCSMC	NCSMC-pheno	R-matrix
$E_r$ (keV)	105	120	65	55	50	47
$\Gamma_r$ (keV)	1100	570	160	110	98	74

Table 1: Energy and width of the  $3/2^+$  resonance derived from the DT eigen-phaseshifts computed within the cluster basis alone, the full NCSMC and the NCSMC-pheno, defined as the energy for which the first derivative of the eigen-phaseshifts is maximal and twice the inverse of the derivative at the resonance energy, respectively. Values derived from R-matrix are shown as reference<sup>48</sup>.

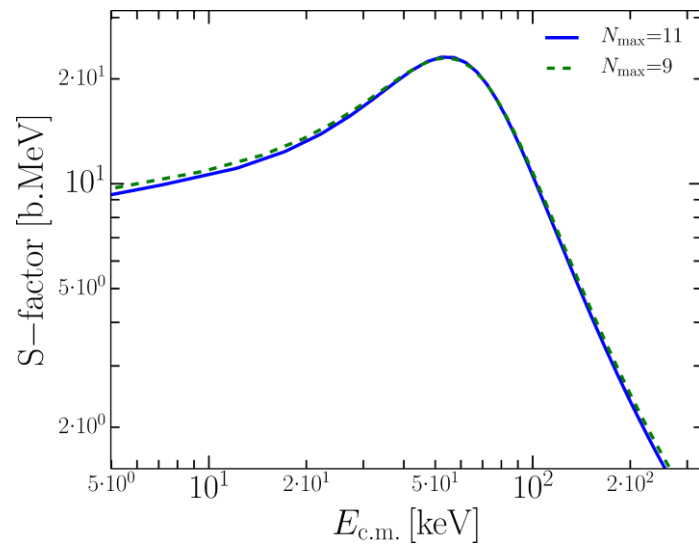


Figure 8: Convergence of the DT S-factor obtained within the NCSMC as a function of the HO model-space size,  $N_{\max}$ . The  $N_{\max} = 11$  many-body basis is currently the largest achievable.

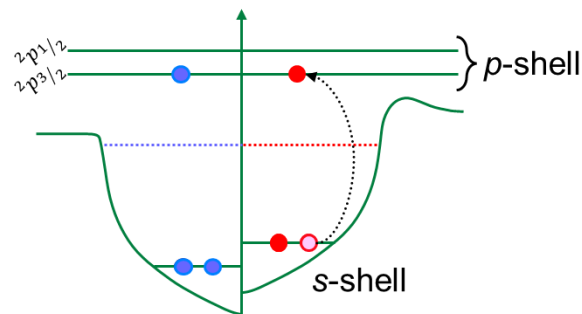


Figure 9: Simple sketch of the structure nature of the  $3/2^+$  resonance; neutrons are in blue and protons in red.

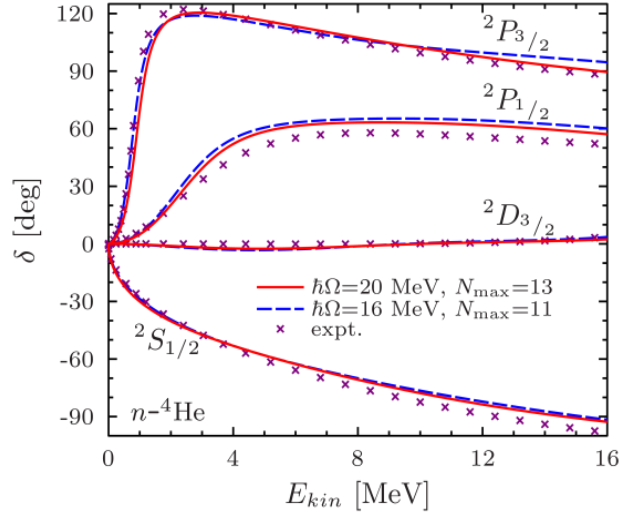


Figure 10: Comparison of the computed  $n + {}^4\text{He}$  phase shifts below the fusion reaction threshold between two sets of NCSMC parameters ( $\hbar\omega = 20 \text{ MeV}$ ,  $\Lambda_{\text{SRG}} = 2.0 \text{ fm}^{-1}$ ,  $N_{\text{max}} = 13$  and  $\hbar\omega = 16 \text{ MeV}$ ,  $\Lambda_{\text{SRG}} = 1.7 \text{ fm}^{-1}$ ,  $N_{\text{max}} = 11$ ). An accurate  $R$ -matrix parametrization of experimental data<sup>46</sup> is shown as a reference (purple crosses).

$N_{\text{max}}$	$\hbar\omega=20 \text{ MeV}, \Lambda_{\text{SRG}}=2.0 \text{ fm}^{-1}$	$\hbar\omega=16 \text{ MeV}, \Lambda_{\text{SRG}}=1.7 \text{ fm}^{-1}$
<b>7</b>	78.70%	42.29%
<b>9</b>	45.04%	18.85%
<b>11</b>	25.68%	8.41%
<b>13</b>	13.78%	-

Table 2: Relative difference with respect to the extrapolated infinite model space result of the eigenvalue of the  ${}^5\text{He} (3/2^+)$  resonance described within the NCSM approach as function of the  $N_{\text{max}}$  parameter.

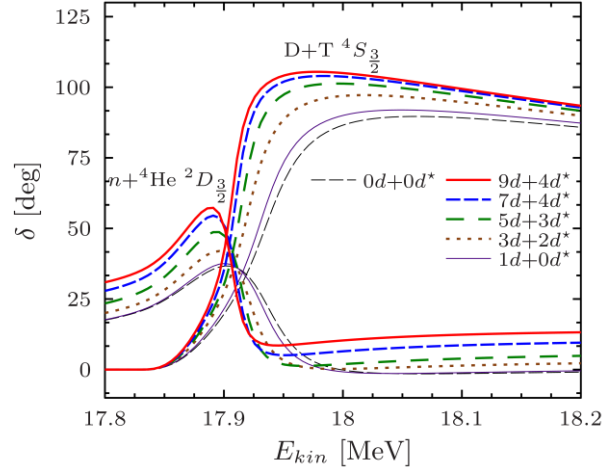


Figure 11: Convergence of the  ${}^4S_{3/2}$   $d$ - ${}^3\text{H}$  and  ${}^2D_{3/2}$   $n$ - $\alpha$  (real part of the) diagonal phase shifts (characterizing, respectively, the entrance and exit scattering states of the DT fusion reaction) in the  $J = 3/2^+$  channel with respect to the number of positive-energy eigenstates of the deuterium projectile, as obtained within the NCSMC approach. We used the notation  $d$  and  $d^*$  for the eigenstates in the  ${}^3S_1$ - ${}^3D_1$  and  ${}^3D_2$  channels of  ${}^2\text{H}$ , respectively.

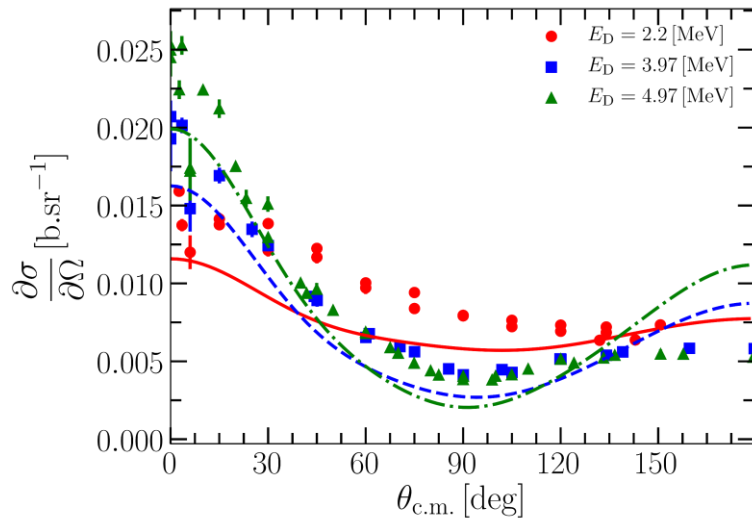


Figure 12: Comparison of the differential cross sections at the deuteron c.m. energies of 2.2 MeV (red solid line), 3.97 MeV (blue dashed line), and 4.97 MeV (green dotted line) computed within the NCSMC with the corresponding experimental data<sup>29,51-54</sup> (symbols).

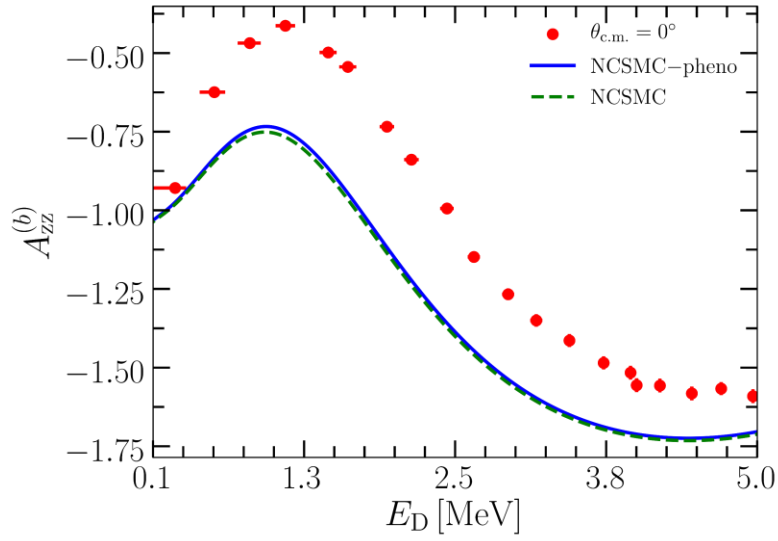


Figure 13: Tensor analyzing power for the DT reaction at energies below the breakup threshold and  $\theta_{\text{c.m.}} = 0^\circ$ . Results obtained within the NCSMC-pheno (blue solid line) and NCSMC (green dashed line) are compared with available experimental data (symbols)<sup>35</sup>.

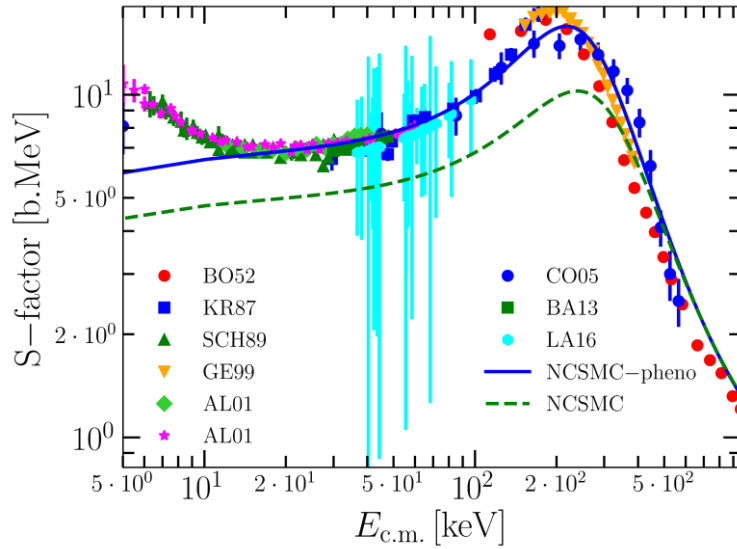


Figure 14:  $D^3\text{He}$  astrophysical S-factor as a function of the energy in the c.m. frame. The result of a  $N_{\text{max}} = 9$  calculation before (green dashed line) and after (blue solid line) phenomenological correction are compared with available nuclear data for the S-factor<sup>36,56-62</sup> (symbols).

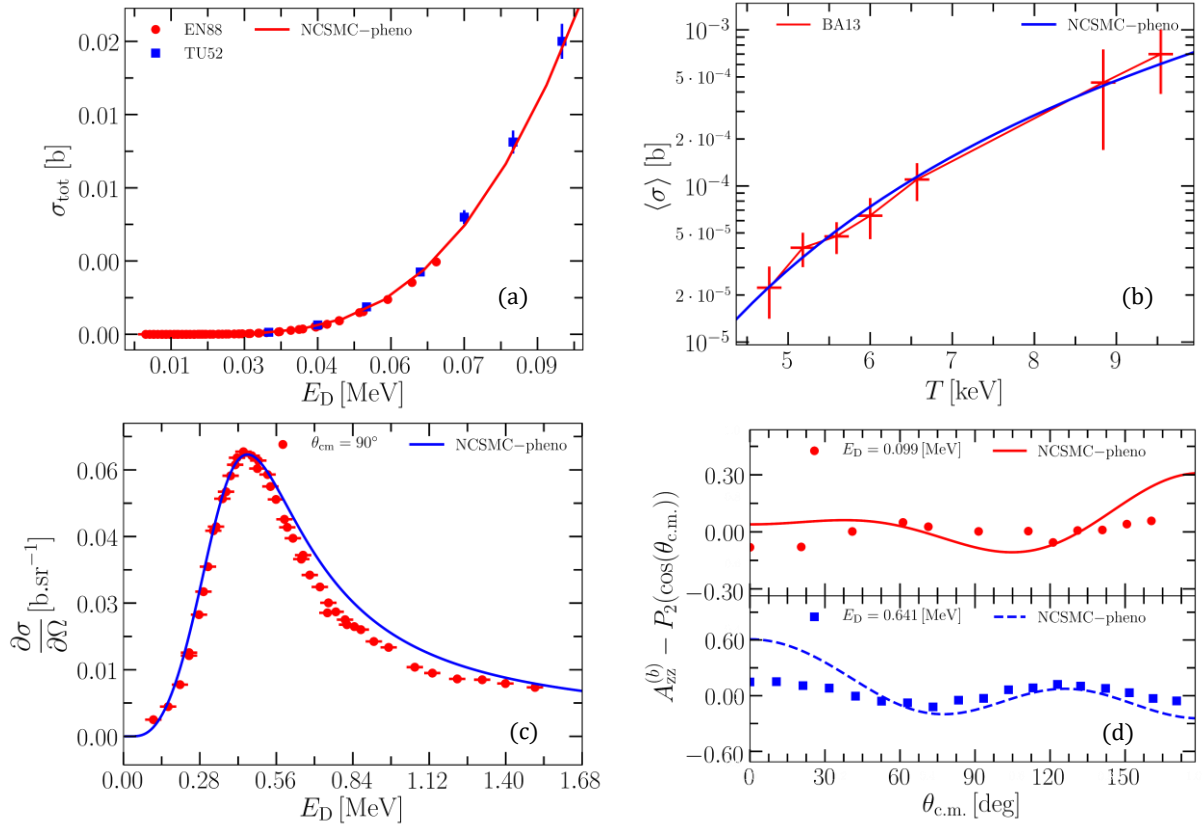


Figure 15: (a) Computed  $D^3\text{He}$  fusion cross section in the energy range below the resonant peak (red solid line) compared to the measurements of refs. 63 (squares) and 64 (circles). (b) Computed  $D^3\text{He}$  temperature averaged cross section (blue solid line) compared to the data of ref. 61 (crosses). (c) Computed  $D^3\text{He}$  differential cross section at  $\theta_{\text{c.m.}} = 90^\circ$  as a function of the impinging deuteron energy (blue solid line) compared to the experimental data of ref. 65 (circles). (d) Computed  $A_{zz}^{(b)}$  tensor analyzing power for the  $D^3\text{He}$  fusion reaction after subtraction of the  $J^\pi = 3/2^+, \ell = 0$  contribution (lines) compared to the data from ref. 36 (symbols) at the D incident energies of  $E_D = 99$  keV (top panel) and 641 keV (bottom panel);

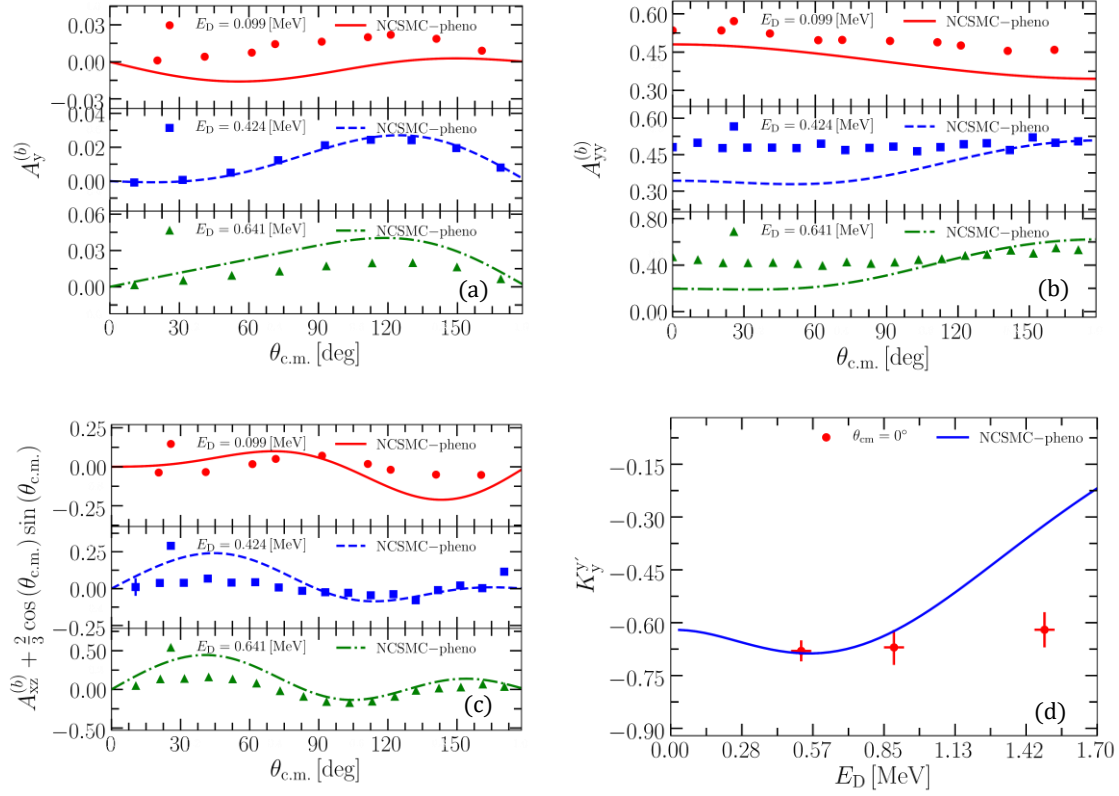


Figure 16: Computed  $D^3\text{He}$   $A_y^{(b)}$  (a),  $A_{yy}^{(b)}$  (b) and  $A_{xz}^{(b)}$  (c) tensor analyzing power for the  $D^3\text{He}$  fusion reaction (lines) compared to the data from ref. 36 (symbols) at the D incident energies of  $E_D = 99$  keV (top panel),  $E_D = 424$  keV (middle panel), and  $641$  keV (bottom panel). The  $J^\pi = 3/2^+$ ,  $\ell = 0$  contribution is subtracted in panel (c). (d) Computed  $D^3\text{He}$  polarization transfer coefficient around the reaction threshold compared to data of ref. 66. Our results include the phenomenological correction.

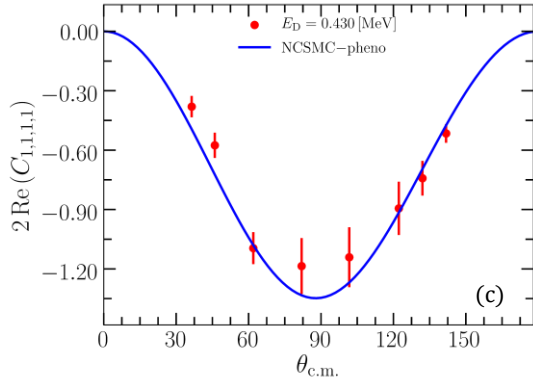
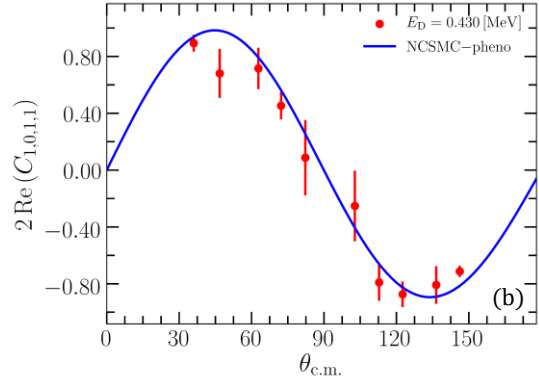
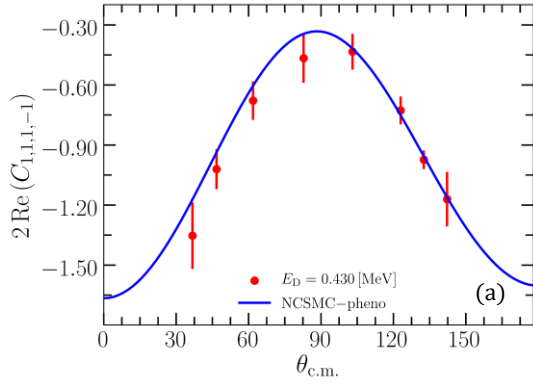


Figure 17: Computed  $D^3\text{He}$   $C_{1,1,1,-1}$  (a),  $C_{1,0,1,1}$  (b) and  $C_{1,1,1,1}$  (c) spherical spin correlation coefficients of the  $D^3\text{He}$  fusion reaction (blue lines) compared to the data from ref. 6 (red symbols) at the D incident energies of  $E_D = 430$  keV. Our results include the phenomenological correction.

## References

1. ITER website: <https://www.iter.org/>.
2. NIF website: <https://lasers.llnl.gov/>.
3. Kulsrud, R.M., Furth, H.P., Valeo, E.J., Goldhaber, M., Fusion Reactor Plasmas with Polarized Nuclei. *Phys. Rev. Lett.* **49**, 1248-1251 (1982).
4. Temporal, M., Brandon, B., Canaud, B., Didelez, J.P., Fedosejevs, R., Ramis, R., Ignition conditions for inertial confinement fusion targets with a nuclear spin-polarized DT fuel. *Nucl. Fusion* **52**, 103011 (2012).
5. Paetz gen. Schieck, H., The status of “polarized fusion”. *Eur. Phys. J. A* **44**, 321-354 (2010).
6. Leemann, Ch., Bürgisser, H., Huber, P., Rohrer, U., Paetz gen. Schieck, H., Seiler, F., Die  $^3\text{He}(d,p)^4\text{He}$  Reaktion mit polarisiertem und unpolarisiertem Target und polarisiertem Deuteronenstrahl bei  $E_d = 430$  keV. *Helv. Phys. Acta* **44**, 141 (1971); *Ann. Phys.* **66**, 810 (1971).
7. Weinberg, S., Nuclear forces from chiral lagrangians. *Phys. Lett. B* **251**, 288–292 (1990).
8. Epelbaum, E., Hammer, H.-W., Meißner, U.-G., Modern theory of nuclear forces. *Rev. Mod. Phys.* **81**, 1773-1825 (2009).
9. Entem, D.R., Machleidt, R., Accurate charge-dependent nucleon-nucleon potential at fourth order of chiral perturbation theory. *Phys. Rev. C* **68**, 041001(2003).
10. Navrátil, P., Local three-nucleon interaction from chiral effective field theory. *Few-Body Syst.* **41**, 117-140 (2007).
11. Gazit, D., Quaglioni, S., Navrátil, P., Three-Nucleon Low-Energy Constants from the Consistency of Interactions and Currents in Chiral Effective Field Theory. *Phys. Rev. Lett.* **103**, 102502 (2009).
12. Hupin, G., Quaglioni, Q., Navrátil, P., Predictive theory for elastic scattering and recoil of protons from  $^4\text{He}$ . *Phys. Rev. C* **90**, 061601 (2014).
13. Hupin, G., Quaglioni, S., Navrátil, P., Unified Description of  $^6\text{Li}$  Structure and Deuterium- $^4\text{He}$  Dynamics with Chiral Two- and Three-Nucleon Forces. *Phys. Rev. Lett.* **114**, 212502 (2015).
14. Baroni, S., Navrátil, P., Quaglioni, S., *Ab initio* Description of the Exotic Unbound  $^7\text{He}$  Nucleus. *Phys. Rev. Lett.* **110**, 022505 (2013).
15. Barrett, B.R., Navrátil, P., Vary, J.P., *Ab initio* no core shell model. *Progr. Part. Nucl. Phys.* **69**, 131-181 (2013).
16. Quaglioni, S., Navrátil, P., *Ab initio* many-body calculations of  $n$ - $^3\text{H}$ ,  $n$ - $^4\text{He}$ ,  $p$ - $^3,^4\text{He}$ , and  $n$ - $^{10}\text{Be}$  scattering. *Phys. Rev. Lett.* **101**, 092501 (2008).
17. Navrátil, P., Quaglioni, S., Hupin, G., Romero-Redondo, S., Calci, A., Unified *ab initio* approaches to nuclear structure and reactions. *Phys. Scripta* **91**, 053002 (2016).
18. Navrátil, P., Quaglioni, S., *Ab initio* Many-Body Calculations of the  $^3\text{H}(d,n)^4\text{He}$  and  $^3\text{He}(d,p)^4\text{He}$  Fusion Reactions. *Phys. Rev. Lett.* **108**, 042503 (2012).
19. Langhammer, J., Navrátil, P., Quaglioni, Q., Hupin, G., Calci, A., Roth, R., Continuum and three-nucleon force effects on  $^9\text{Be}$  energy levels. *Phys. Rev. C* **91**, 021301 (2015).
20. Calci, A., Navrátil, P., Roth, R., Dohet-Eraly, J., Quaglioni, S., Hupin, G., Can *Ab initio* Theory Explain the Phenomenon of Parity Inversion in  $^{11}\text{Be}$ ? *Phys. Rev. Lett.* **117**, 242501 (2016).
21. Otsuka, T., Suzuki, T., Holt, J.D., Schwenk, A., Akaishi, Y.i., Three-Body Forces and the Limit of Oxygen Isotopes. *Phys. Rev. Lett.* **105**, 032501 (2010).

22. Cipollone, A., Barbieri, C., Navrátil, P., Isotopic Chains Around Oxygen from Evolved Chiral Two- and Three-Nucleon Interactions. *Phys. Rev. Lett.* **111**, 062501 (2013).
23. Hagen, G., Hjorth-Jensen, M., Jansen, G.R., Machleidt, R., Papenbrock, T., Continuum effects and three-nucleon forces in neutron-rich oxygen isotopes. *Phys. Rev. Lett.* **108**, 242501 (2012).
24. Navrátil, P., Gueorguiev, V. G., Vary, J. P., Ormand, W. E., Nogga, A., Structure of A=10–13 Nuclei with Two- Plus Three-Nucleon Interactions from Chiral Effective Field Theory. *Phys. Rev. Lett.* **99**, 042501 (2007).
25. Liskien, H., Paulsen, A. *Atomic Data and Nuclear Data Tables* **11**, 569-619 (1973).
26. Conner, J.P., Bonner, T.W., Smith, J.R., A Study of the  ${}^3\text{H}(d,n){}^4\text{He}$  Reaction. *Phys. Rev.* **88**, 468-473 (1952).
27. Arnold, W.R., Phillips, J.A., Sawyer, G.A., Stovall, E.J. Jr., Tuck, J.L., Cross Sections for the Reactions  $\text{D}(d, p)\text{T}$ ,  $\text{D}(d, n){}^3\text{He}$ ,  $\text{T}(d, n){}^4\text{He}$ , and  ${}^3\text{He}(d, p){}^4\text{He}$  below 120 keV. *Phys. Rev.* **93**, 483-497 (1954).
28. Brown, R.E., Jarmie, N., Hale, G.M., Fusion-energy reaction  ${}^3\text{H}(d,\alpha)n$  at low energies. *Phys. Rev. C* **35**, 1999-2004 (1987).
29. Otuka, N., et al. Nuclear Data Sheets **120**, 272-276 (2014).
30. Drogg, M., Otuka, N., Evaluation of the absolute angle-dependent differential neutron production cross sections by the reactions  ${}^3\text{H}(p,n){}^3\text{He}$ ,  ${}^1\text{H}(t,n){}^3\text{He}$ ,  ${}^2\text{H}(d,n){}^3\text{He}$ ,  ${}^3\text{H}(d,n){}^4\text{He}$ , and  ${}^2\text{H}(t,n){}^4\text{He}$  and of the cross sections of their time-reversed counterparts up to 30 MeV and beyond. INDC(AUS)-0019 (2015).
31. Ohlsen, G.G., Polarization transfer and spin correlation experiments in nuclear physics. *Rep. Progr. Phys.* **35**, 717 (1972).
32. Paetz gen. Schieck, H., Nuclear physics with polarized particles. *Lecture Notes in Physics* **842**, Springer (2012).
33. Przewoski, B. v., et al., Analyzing powers and spin correlation coefficients for p+d elastic scattering at 135 and 200 MeV. *Phys. Rev. C* **74**, 064003 (2006).
34. Bém, P., Kroha, V., Mareš, J., Šimečková, E., Trgiňová, M., Verčimák, P., Angular Anisotropy of the  ${}^3\text{H}(d,\alpha)n$  Reaction at Deuteron Energies Below 200 keV. *Few-Body Syst.* **22**, 77-89 (1997).
35. Dries, L.J., Clark, H.W., Detomo R. Jr., Regner, J.L., Donoghue, T.R.,  $A_{zz}(0^\circ)$  for the charge-symmetric  ${}^3\text{He}(\vec{d},p){}^4\text{He}$  and  ${}^3\text{H}(\vec{d},n){}^4\text{He}$  reactions below 6.75 MeV. *Phys. Rev. C* **21**, 475-482 (1980).
36. Geist, W.H., Brune, C.R., Karwowski, H.J., Ludwig, E.J., Veal, K.D., Hale, G.M., The  ${}^3\text{He}(\vec{d},p){}^4\text{He}$  reaction at low energies. *Phys. Rev. C* **60**, 054003 (1999).
37. Thompson, I.J., Nunes, F.M., Nuclear Reactions for Astrophysics. Cambridge university press (2009).
38. Bosch H.-S., Hale, G.M., Improved formulas for fusion cross-sections and thermal reactivities. *Nucl. Fusion* **32**, 611-631 (1992).
39. Descouvemont, P., Adahchoura, A., Angulo, C., Coc, A., Vangioni-Flam, E., Compilation and R-matrix analysis of Big Bang nuclear reaction rates. *Atomic Data and Nuclear Data Tables* **88**, 203-236 (2004).
40. C. Angulo *et al.*, A compilation of charged-particle induced thermonuclear reaction rates. *Nucl. Phys. A* **656** 3-187 (1999).

41. Dohet-Eraly, J., Navrátil, P., Quaglioni, S., Horiuchi, W., Hupin, G., Raimondi, F.,  ${}^3\text{He}(\alpha,\gamma){}^7\text{Be}$  and  ${}^3\text{H}(\alpha,\gamma){}^7\text{Li}$  astrophysical S-factors from the no-core shell model with continuum. *Phys. Lett. B* **757**, 430-436 (2016).
42. Romero-Redondo, C., Quaglioni, S., Navrátil, P., Hupin, G., How Many-Body Correlations and  $\alpha$  Clustering Shape  ${}^6\text{He}$ . *Phys. Rev. Lett.* **117**, 222501 (2016).
43. Elhatisari, S., Lee, D., Rupak, G., Epelbaum, E., Krebs, H., Lähde, T.A., Luu, T., Meißner, U.-G., *Ab initio* alpha-alpha scattering. *Nature* **528**, 111-114 (2015).
44. Descouvemont, P., Baye, D., The R-matrix theory. *Rep. Progr. Phys.* **73**, 036301 (2010).
45. Baye, D., The Lagrange-mesh method. *Phys. Rep.* **565**, 1–107 (2015).
46. Hale, G.M. Private communication.
47. Hupin, G., Langhammer, J., Navrátil, P., Quaglioni, S., Calci, A., Roth, R., *Ab initio* many-body calculations of nucleon- ${}^4\text{He}$  scattering with three-nucleon forces. *Phys. Rev. C* **88**, 054622 (2013).
48. Hale, G.M., Brown, R.E., Jarmie, N., Pole structure of the  $J^\pi = 3/2^+$  resonance in  ${}^5\text{He}$ . *Phys. Rev. Lett.* **59**, 763-766 (1987).
49. Haesner, B., Heeringa, W., Klages, H.O., Dobiash, H., Schmalz, G., Schwarz, P., Wilczynski, J., Zeitnitz, B., Measurement of the  ${}^3\text{He}$  and  ${}^4\text{He}$  total neutron cross sections up to 40 MeV, *Phys. Rev. C* **28**, 995 (1983).
50. Nollett, K.M., Pieper, S.C., Wiringa, R.B., Carlson, J., Hale, G.M., Quantum Monte Carlo Calculations of Neutron-  $\alpha$  Scattering. *Phys. Rev. Lett.* **99**, 022502 (2007).
51. Galonsky, A., Johnson, C.H., Cross Sections for the  $\text{T}(d,n){}^4\text{He}$  Reaction. *Phys. Rev.* **104**, 421-425 (1956).
52. Bame, S.J. Jr., Perry, J.E. Jr.,  $\text{T}(d, n){}^4\text{He}$  Reaction. *Phys. Rev.* **107**, 1616-1620 (1957).
53. McDaniels, D.K., Drogg, M., Hopkins, J.C., Seagrave, J.D., Angular Distributions and Absolute Cross Sections for the  $\text{T}(d,n){}^4\text{He}$  Neutron-Source Reaction. *Phys. Rev. C* **7**, 882 (1973).
54. Brill', O.D., Pankratov, V.M., Rudakov, V.P., Rybakov, B.V., Neutron production cross sections and energies for the reactions  $\text{T}(p,n){}^3\text{He}$ ,  $\text{D}(d,n){}^3\text{He}$ , and  $\text{T}(d,n){}^4\text{He}$ . *Sov. Atom. En.* **16**, 161 (1964).
55. Tilley, T.R., Cheves, C.M., Godwin, J.L., Hale, G.M., Hofmann, H.M., Kelley, J.H., Sheu C.G., Weller, H.R., Energy levels of light nuclei  $A=5, 6, 7$ . *Nucl. Phys. A* **708**, 3-163 (2002).
56. Bonner, T.W., Conner, J.P., Lillie, A.B., Cross Section and Angular Distribution of the  ${}^3\text{He}(d,p){}^4\text{He}$ . *Phys. Rev.* **88**, 473 (1952).
57. Krauss, A., Becker, H.W., Trautvetter, H.P., Rolfs, C., Brand, K., Low-energy fusion cross sections of  $\text{D}+\text{D}$  and  $\text{D}+{}^3\text{He}$  reactions. *Nucl. Phys. A* **465**, 150-172 (1987).
58. Schröder, U., Engstler, S., Krauss, A., Neldner, K., Rolfs, C., Somorjai, E., Langanke, K., Search for electron screening of nuclear reactions at sub-coulomb energies. *Nucl. Instrum. Methods Phys. Res. B* **40–41**, 466-469 (1989).
59. Aliotta, M., et al., Electron screening effect in the reactions  ${}^3\text{He}(d, p){}^4\text{He}$  and  $\text{d}({}^3\text{He}, p){}^4\text{He}$ . *Nucl. Phys. A* **690**, 790-800 (2001).
60. La Cognata, M., et al., Bare-nucleus astrophysical factor of the  ${}^3\text{He}(d,p){}^4\text{He}$  reaction via the “Trojan horse” method. *Phys. Rev. C* **72**, 065802 (2005).
61. Barbui, M., et al., Measurement of the Plasma Astrophysical S Factor for the  ${}^3\text{He}(d,p){}^4\text{He}$  Reaction in Exploding Molecular Clusters. *Phys. Rev. Lett.* **111**, 082502 (2013).
62. Lattuada, D., et al., Model-independent determination of the astrophysical S factor in laser-induced fusion plasmas. *Phys. Rev. C* **83**, 045808 (2016).

63. Arnold, W.R., Phillips, J.A., Sawyer, G.A., Stovall, E.J., Tuck, J.L., Cross Sections for the Reactions  $D(d, p)T$ ,  $D(d, n)^3\text{He}$ ,  $T(d, n)^4\text{He}$ , and  $^3\text{He}(d, p)^4\text{He}$  below 120 keV. *Phys. Rev.* **93**, 483 (1954).
64. Engstler, S., Krauss, A., Neldner, K., Rolfs, C., Schröder, U., Langanke, K., Effects of electron screening on the  $^3\text{He}(d, p)^4\text{He}$  low-energy cross sections. *Phys. Lett. B* **202**, 179-184 (1988).
65. Klucharev, A.P., Eselson, B.N., Val'ev, A.K., Study of  $^3\text{He}$  reaction with deuterons. *Sov. Phys.-Doklady* **1**, 475 (1956).
66. Fletcher, K.A., et al.,  $K_y^{y'}$  ( $0^\circ$ ) for  $^3\text{He}(d,p)^4\text{He}$  near the  $J^\pi = \frac{3}{2}^+$  resonance. *Phys. Rev. C* **66**, 057601 (2002).

## **Acknowledgements, Author Contribution and Competing financial interests**

### **Acknowledgements**

Computing support for this work came from the Lawrence Livermore National Laboratory (LLNL) institutional Computing Grand Challenge program. This article was prepared by LLNL under Contract DE-AC52-07NA27344. This material is based upon work supported by the U.S. Department of Energy, Office of Science, Office of Nuclear Physics, under Work Proposals No. SCW1158 and SCW0498, and by the Natural Sciences and Engineering Research Council of Canada (NSERC) Grants No. SAPIN-2016-00033. TRIUMF receives funding via a contribution through the Canadian National Research Council of Canada.

### **Author Contributions**

G.H. carried out the calculations in consultation with S.Q. and P.N. All authors discussed the results and contributed to the manuscript at all stages.

### **Competing financial interests**

The authors declare no competing financial interests.

### **Author information**

Correspondence and requests for materials should be addressed to [hupin@ipno.in2p3.fr](mailto:hupin@ipno.in2p3.fr)